GEOPHYSICS, VOL. 69, NO. 4 (JULY-AUGUST 2004); P. 885–897, 10 FIGS., 1 TABLE.
10.1190/1.1778232

Downloaded 11/03/15 to 130.56.64.29. Redistribution subject to SEG license or copyright; see Terms of Use at http://library.seg.org/

Pressure-dependent seismic response of fractured rock

Evgenii A. Kozlov*

ABSTRACT

Effects of external stress and pore pressure variations on the seismic signature of fractured rocks remain of interest to geoscientists and practicing geophysicists. Commonly, the effects are modeled theoretically, assuming fracture faces to be rough surfaces contacting each other via the surface asperities. The model proposed here differs from other models of this kind in that (1) fracture roughness is described by a single parameter and (2) a controlled degree of hydraulic connectivity between fractures and equant pores is introduced. This adds to the model's convenience and makes it applicable to a wide variety of reservoirs. The model predictions of seismic velocities in fractured rock at variable stress are consistent with experimental data. For fixed effective stress, the model predictions coincide with those obtained using the model with ellipsoidal fractures of certain average aspect ratio and the same fracture porosity.

Apart from known effects, the model introduced predicts an amplification of the stress variation influence on fracturing-induced anisotropy with an increase of connected equant porosity, a decrease of V_P/V_S with effective stress, and implicit frequency dependence of the V_P/V_S relation. It is also shown that amplitude versus offset (AVO) anomalies caused by fluid replacement can be seriously distorted if the fluid replacement is accompanied by significant variations of pore pressure, as, for example, at intense gas production. Neglecting these effects can lead to erroneous conclusions on shear modulus dependence on the pore fluid type. Qualitatively, in rocks with azimuthally aligned fracturing, the increase of effective stress affects AVO gradient in about the same way as the increase of water saturation parameter S_w. In contrast, the AVO intercept is not affected by variations of effective stress, while fluid replacement effect on the intercept is significant. Potentially, this can help distinguish the effects of pore pressure variations and fluid replacement on the AVO attributes.

INTRODUCTION

In the seismic frequency range, aligned fracturing of rocks manifests itself in the form of anisotropy of P- and S-wave velocities and consequent anisotropy of reflectivity. Since the origin and evolution of such fracturing is commonly controlled by pore pressure and/or lithostatic stress, it is of interest to establish a theoretical relationship between effective stress and seismic signature of fracturing.

The most common type of fractured rock models is a homogeneous medium with ellipsoidal (penny-shaped) inclusions imitating fractures (O'Connell and Budiansky, 1977; Hudson, 1981; Thomsen, 1995). Effects of pressure variation on elastic properties of rocks with interconnected ellipsoidal fractures and pores are described by Hudson et al. (1996), Hudson (2000), and Liu et al. (2001). Yet in models with aligned uniform ellipsoidal fractures, the fracture-induced compliance does not decrease as the fracture openings decrease with stress, which is unnatural. The compliance decrease can be modeled by reducing the number of nonuniform fractures, but it is rather complicated. An alternative description of the compliance dependence on stress results in models with rough-face fractures.

In such models, fractures are treated as thin, nominally flat contact layers (Kragelskii, 1965; Greenwood and Williamson, 1966; Gangi, 1981; White, 1983; Boitnott et al., 1992; Gangi and Carlson, 1996; Kozlov, 1997) or inclusions (Pecorari, 1997) with rough nonconforming boundaries—fracture faces, contacting each other via asperities on opposite faces.

The model response of a fracture to increasing compressive stress is essentially the increase of the area of direct contact of fracture faces via their asperities. To comply with observations of fracture face microtopography, the tips of asperities are commonly assumed to be spherical (Kragelsky, 1965; Greenwood and Williamson, 1966; White, 1983; Pecorari, 1997; Kozlov and Varivoda, 2000). Also, the asperity heights are allowed to vary according to an exponential, Gaussian, or power distribution law to account for the observed approximate linearity (Greenwood and Williamson, 1966; Gangi and Carlson,

Published on Geophysics Online April 5, 2004. Manuscript received by the Editor August 4, 2002; revised manuscript received October 27, 2003.
*Paradigm Geophysical, B.V., 1st Golutvinsky Pereulok 1, Moscow 119180, Russia, E-mail: evgeniko@paradigmgeo.com.
© 2004 Society of Exploration Geophysicists. All rights reserved.

Downloaded 11/03/15 to 130.56.64.29. Redistribution subject to SEG license or copyright; see Terms of Use at http://library.seg.org/

1996) of total surface of asperity contacts in stress. The fracture face roughness in such models is described by three or four parameters that can be varied arbitrarily to ensure a good fit of the model dependencies to observed data. The most flexible model is the bed of nails (Kragelskii, 1965; Gangi, 1981): it imitates distribution of asperity shapes by a mechanically equivalent distribution of heights of elastic rods (nails). However, to use such highly flexible models for theoretical studies, one must first define the ranges of its three or four parameters, i.e., define a certain initial model.

Creating of such an initial model is the starting point of this paper. The proposed model differs from other rough-face models in that (1) the roughness is described not by distributions of asperity heights and radii but by a single parameter – the average normalized distance between neighbor contacts, as in Kozlov (1997) and Kozlov and Varivoda (2000)—and (2) connected equant porosity is ascribed to the host rock. Despite its simplicity, the model serves its purpose rather well. In addition to known effects, it predicts amplification in the effect of stress on velocities in fluid-saturated rocks with the increase of connected equant porosity, predicts the decrease of relation V_P/V_S with the stress, and helps clarify the not uncommon situation when dependency of shear modulus on pore pressure is misinterpreted as dependency of the rock shear modulus on the pore fluid type, when fluid substitution in a real reservoir is accompanied by alteration of pore pressure.

The model assumes strictly parallel fractures. Effective compliances and wave velocities are considered only for raypath trajectories parallel and normal to fracture planes. Bulk modulus of gaseous pore fluid is assumed negligible compared to rock bulk modulus. These are the same restrictions that cause misinterpretation (Hudson and Crampin, 2003) of observed data by van der Kolk et al. (2001). Hence, quantitative estimates that can be obtained using the introduced model should be related to in-situ rocks with caution.

In the first section of the paper, the model formalism is presented, and the effective stress dependence of fractured rock compliance and velocity is considered. Then, the model is expanded to an orthorhombic medium with vertically aligned fracture-induced horizontal transverse isotropy (HTI) imposed on a vertical transverse isotropy (VTI) of the host rock with nonzero equant porosity. Further, expressions for the effective pressure-dependent Thomsen's anisotropy coefficients and reflectivity are derived for the expanded model. Finally, some numerical results are considered, and the possibility of inverting estimates of azimuth-dependent anisotropy coefficients and amplitude versus offset (AVO) attributes for lateral variations of pressure, saturation, and connected equant porosity is discussed.

MODEL FORMULATION

Rough-face fractures with stress-dependent compliance

In a fracture with rough, nonconforming faces contacting each other via asperities, the reference surfaces of the faces are assumed parallel, and asperities in contact are represented by uniform hemispheres of radius R. Asperity contacts are parallel to the reference surfaces. Average distance l between centers of neighbor asperities on each face is defined as $2cR$ (Figure A-1). For rough face fractures, the value $1/c$ plays the same role as the aspect ratio for ellipsoidal fractures. The value l is assumed to be much smaller than fracture size. A set of such fractures parallel to each other forms a fracture system described by its orientation and fracture density. Fracture density is roughly defined as

$$e = \frac{2R}{L}, \tag{1}$$

where $2R$ is a nominal distance between fracture face reference surfaces and $L \gg 2R$ is the average distance between fractures (Figure A-1).

Relation (1) virtually coincides with Schoenberg's (1983) definition of fracture density for a linear slip interface model represented by the alternation of soft and hard layers, but it deviates from the definition of ellipsoidal fracture density (number of fractures per unit surface or volume). Yet in lithologically homogeneous rocks, for which the average size R of asperities on fracture faces can be assumed spatially invariant, variation of the fracture density [equation (1)] does characterize the variation of the number of fractures per unit length in the direction normal to the fracture faces. During seismic wave propagation, only hydraulic interaction between fractures is considered.

According to Schoenberg and Sayers (1995), a system of such fractures introduces to the rock an additional compliance that can be unambiguously expressed via its two components, Z_N and Z_T, normal and tangential to the fracture faces. For fluid-saturated fractures, hydraulically connected with equant pores of the host rock, Hertz/Mindlin's formalism of contacting spheres (Appendix A), combined with Thomsen's approach to hydraulic connectivity between fractures and pores (Appendix B), leads to

$$Z_T \equiv \frac{1}{\tilde{\mu}} - \frac{1}{\mu} = ce\,(1-0.5\nu^*)\sqrt[3]{\frac{2c}{3}\frac{1}{(1-\nu^*)\mu^2 p}}, \tag{2a}$$

$$Z_N \equiv \frac{1}{\tilde{K}} - \frac{1}{K} = \frac{2}{3}ce\left(1-\frac{K_f}{K_s}\right)\sqrt[3]{c\frac{(1-\nu^{*2})^2}{(1-2\nu^*)^2}\frac{1}{K^{*2}p}}\cdot D, \tag{2b}$$

where $D = ((\phi+\phi_c)/\phi_p)D_1 + (\phi_p-\phi-\phi_c)/\phi_p)D_2$ is the so-called fluid influence factor (Thomsen, 1995):

$$D_1 = \left\{1 - \frac{K_f}{K_s} + \frac{K_f}{\phi K^*}\left[\left(1-\frac{K^*}{K_s}\right) + \frac{2}{3}c\,e\cdot\sqrt[3]{\frac{c}{3}\frac{(1-\nu^{*2})^2}{(1-2\nu^*)^2}\frac{K^*}{p}}\right]\right\}^{-1}, \tag{3a}$$

and

$$D_2 = \left\{1 - \frac{K_f}{K_s} + \frac{2}{3}\frac{K_f}{K^*}\left[\frac{\left(1-\frac{K_f}{K_s}\right)}{\left(1-\frac{K_f}{K}\right)}\frac{c\,e}{\phi_c} \times\sqrt[3]{\frac{c}{3}\frac{(1-\nu^{*2})^2}{(1-2\nu^*)^2}\frac{K^*}{p}}\right]\right\}^{-1}. \tag{3b}$$

Here, $p = p_0 + p_1 - np_f$ is the effective stress component normal to fracture faces, where p_0 is the confining stress component normal to fracture faces, $p_1 \geq 0$ reflects the effect of rock

Downloaded 11/03/15 to 130.56.64.29. Redistribution subject to SEG license or copyright; see Terms of Use at http://library.seg.org/

cohesiveness (Gangi, 1981), p_f is pore pressure, and n is the effective stress coefficient. Further, K and μ are bulk and shear moduli of unfractured (intact) rock, ν is its Poisson coefficient, and K_s and K_f are the rock mineral and pore fluid bulk moduli, respectively. In the definition of quantity D, ϕ_p is total porosity, ϕ is the connected portion of equant porosity (pores are hydraulically connected with each other and with fractures), and ϕ_c is fracture porosity, so the disconnected portion of equant porosity is $\phi_p - \phi - \phi_c$. For the rock moduli, an asterisk as a superscript means a dry state of intact rock, and a bar over a designation means fractured, fluid-saturated rock.

In equations (2) and (3), as in the models with ellipsoidal (penny-shaped) fractures, the fracturing-induced extra compliance is linear in fracture density. A specific feature of the proposed model is strong dependence of the extra compliance on fracture face roughness parameter c and explicit dependence on effective pressure p. Another peculiarity of the model [equations (1)–(3)] is effective stress dependence of relation Z_T/Z_N as a result of the stress dependence of factor D, [equations (3)]. Note the scale invariance of the model [equations (2 and 3); it does not depend on any of the values R, l, and L.

Stress-independent prototypes of expressions (3) for D_1 and D_2 as particular cases of the fluid influence factor D are derived in Thomsen (1995) for a pressure-independent model with ellipsoidal fractures. The prototypes were related to low (surface seismic) and moderately high frequency ranges, respectively. The difference between these frequency ranges is, after Thomsen, that when low-frequency waves propagate, the pore pressure in cracks and equant pores has time to equilibrate because of fluid flow between the voids; while at moderately high frequencies, equilibration does not exist because there is no such flow. Here, quantities D_1 and D_2 are related to connected and disconnected portions of equant porosity, both in the seismic frequency range. It means that fluid influence factor D is frequency dependent: at frequencies defined by Thomsen (1995) as moderately high, the influence of all the equant porosity is described by equation (3b).

The proposed model provides no internal threshold to distinguish between fracture and equant porosity. Qualitatively, voids with the roughness parameter $c \approx 1$ to 3 may be regarded as equant pores, while voids with $c \geq 3$ sparsely distributed in the rock volume ($2R/L < 0.1$) may be defined as fractures. The inequality for c is equivalent to inequality $A \leq 1\%$ stated in Greenwood and Williamson (1966), where A is the relative area of asperity contacts and inequality for $2R/L$ stems from the fracture criticality concept (Crampin, 1994).

The proposed model [equations (2), (3)] implies a certain dependence of rock porosity on the effective stress p. For pore space geometry as shown in Figure A-1, fracture porosity is

$$\phi_c = \frac{e[1-0.64c^{-2}(1-3\xi^2)-\xi]}{1-e\xi} \approx e(1-0.64c^{-2}-\xi),$$

$$p_1 < p < E^*\left\{\frac{[1-0.64c^{-2})]^{3/2}}{7c^2(1-\nu^2)}\right\} \qquad (4)$$

(Appendix C), where the stress-induced relative decrease ξ of initial fracture opening is defined by equation (A-3).

Since the distance between reference surfaces of fracture faces is stress dependent, fracture density as defined in the model is also weakly stress dependent. So with account to equation (4),

$$e^{exact} = \frac{2R(1-\xi)}{L} = e(1-\xi), \quad \xi \ll 1. \qquad (5)$$

Using relation (4), fracture density e in equations (2) can be replaced by fracture porosity ϕ_c, which seems to be a more appropriate parameter for reservoir characterization than e. Compliances Z_N and Z_T are then seen to be linear in fracture porosity . Note that by analogy with the pore space compressibility (e.g., Mavko and Mukerji, 1995), the dry compliance Z_N can be thought of as a fracture space compressibility factored by fracture porosity ϕ_c.

At fracture closing, the parameter c is intuitively expected to decrease, and vice versa. Taking account of experimental data, it is reasonable (Appendix D) to use a power law form of the roughness factor c stress dependence:

$$c = c_0\left(\frac{p_1}{p}\right)^m, \quad 0.2 \leq m \leq 0.35. \qquad (6a)$$

Equation (6a) implies an experiment-consistent increase of average aspect ratio of fractures with stress p (Figure 1). The model-defined theoretical upper limit is $m < 0.5$; when m approaches 0.5, the rate of decrease of the fracture faces' separation ξ with p aproaches zero. Simultaneously, the rate of growth of the total area of asperity contacts with stress approaches (from below) linearity in p (Appendix D). In

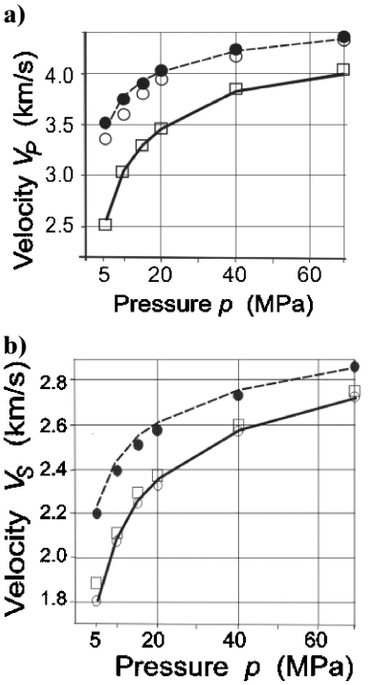

Figure 1. Model (lines) and measured [circles and boxes; Sayers (2002)] velocities as functions of stress. Solid lines are for either propagation or polarization perpendicular to fracture planes, and dashed lines are for both propagation and polarization parallel to fracture planes. Note reasonable agreement between modeled and measured data. (a) Measured P-wave velocities V_{11} (•), V_{22} (○), and V_{33} (□). (b) Measured S-wave velocities $V_{12} = V_{21}$ (•), $V_{13} = V_{31}$ (○), and $V_{23} = V_{32}$ (□). The fracturing-affected velocities are V_{33} and $V_{23} = V_{32}$.

Downloaded 11/03/15 to 130.56.64.29. Redistribution subject to SEG license or copyright; see Terms of Use at http://library.seg.org/

experiments, the latter limit is also approached from below (Kragelskii and Mikhlin, 1984; Gangi and Carlson, 1996), which implicitly validates the model. Note that at any fixed stress p value, roughness c remains to be a single fracture microtopography parameter defining its compliance, as in the stress-dependent aspect ratio of ellipsoidal cracks.

Setting constrains

$$3 \le c_0, \quad 0 \le e \le 0.1 \tag{6b}$$

as arbitrary reasonable limits completes the model definition.

Stress-dependent anisotropy

For a single system of vertically aligned fractures inducing HTI to the rock, the stress component p_0, normal to fracture faces, is the minimum of two principal horizontal components of lithostatic stress. To make the model applicable to a wide variety of siliciclastic rocks, the host rock is assumed to have a VTI symmetry, which leads to orthorhombic symmetry of the model (Shoenberg and Helbig, 1997). In the case of bedding-concordant fracturing (e.g., Vernik, 1993), the anisotropy introduced by such fracturing is included in the VTI component. In the simplified form of negligible VTI component, the model is applicable to fractured carbonate rocks. The only stress-dependent component of the model is assumed to be the HTI anisotropy on account of aligned vertical fractures with rough faces.

According to Liu et al. (1996) and Kozlov (1997), model (1), (2) belongs to the class of models based on the linear slip theory (Schoenberg, 1983). In the framework of this theory and the weak anisotropy assumption (Thomsen, 1986), the Thomsen's effective anisotropic coefficients ε, δ, and γ of the orthorhombic model should represent the sums of the VTI background components ε_b, δ_b, and γ_b, and the anisotropy coefficients ε_f, δ_f, and γ_f of the HTI medium, resulting from aligned fractures in an imaginary isotropic host rock sufficiently close to the VTI background model (Bakulin et al., 2000):

$$\varepsilon = \varepsilon_b + \varepsilon_f, \tag{7a}$$

$$\delta = \delta_b + \delta_f, \tag{7b}$$

$$\gamma = \gamma_b + \gamma_f. \tag{7c}$$

Here, for convenience, both the background and fracture-induced anisotropy coefficients are defined with respect to the vertical axis, which is the axis of symmetry for VTI background only. The coefficients ε_f, δ_f, and γ_f are azimuth dependent, while ε_b, δ_b, and γ_b are not.

In the case of seismic-wave propagation in the HTI isotropy (ISO) plane, normal to the HTI axis of symmetry,

$$\varepsilon_f = \delta_f = \gamma_f = 0, \tag{8}$$

so anisotropy of the effective model as a whole is reduced to anisotropy of the background. In the direction parallel to HTI axis of symmetry (SYM), absolute values of coefficients ε_f, δ_f, and γ_f are maximal.

For a rock containing a rotationally invariant system of aligned ellipsoidal cracks, Schoenberg (1994) expresses Thomsen's generic (i.e., those defined with respect to the HTI axis of symmetry here) anisotropy coefficients $\varepsilon'_f\delta'_f$, γ'_f via fracturing-induced additional compliances Z_N and Z_T. Applying these expressions to the model with rough-face fractures as a version of linear slip interface media, and using equations (2) and (3), derived for the stress-dependent compliances Z_N and Z_T, yields (Appendix E)

$$\varepsilon'_f = \left(\frac{1-\nu^{*2}}{1-2\nu^*}\right)^{2/3} \frac{1-2\nu}{1-\nu^2}\left(1-\frac{K_f}{K_s}\right) c^{4/3} e \frac{K}{K^*} \times \sqrt[3]{\frac{K^*}{p}} \cdot D, \tag{9a}$$

$$\gamma'_f = \frac{(2-\nu^*)(1-2\nu)}{4[(1-\nu^{*2})(1-2\nu^*)^2]^{1/3}} c^{4/3} e \frac{K}{K^*} \sqrt[3]{\frac{K^*}{p}}, \tag{9b}$$

$$\delta'_f = 2(1-\nu)\varepsilon'_f - 2\left(\frac{1-2\nu}{1-\nu}\right)\gamma'_f. \tag{9c}$$

Coefficients ε_f, δ_f, and γ_f, defined with respect to the VTI axis of symmetry, are expressed via $\varepsilon'_f\delta'_f$, and γ'_f values using Tsvankin's (1997) relations between the two sets of coefficients, which in linear approximation read

$$\alpha_f \approx -\alpha'_f; \quad \alpha = \varepsilon_f, \delta_f, \gamma_f; \quad a'_f = \varepsilon'_f, \delta'_f, \gamma'_f. \tag{9d}$$

Stress-dependent reflectivity

To connect static stress with reflectivity, I use an approximate expression for reflection coefficient of a boundary between two VTI half-spaces and analogous expression for two HTI half-spaces with the same direction of HTI axis of symmetry (Ruger, 1998). Combining these expressions in accord with equations (7) yields, for a precritical angle of incidence θ and an arbitrary angle ψ between the HTI axis of symmetry and offset orientation,

$$R_{PP}(\theta,\psi) = \frac{1}{2}\frac{\Delta I}{I} + \frac{1}{2}\left\{\frac{\Delta V_P}{\bar{V}_P} - 4G\frac{\Delta\mu}{\bar{\mu}} + \Delta\delta_b + [\Delta\delta_f + 8G\Delta\gamma_f]\cos^2\psi\right\}\sin^2\theta + \frac{1}{2}\left\{\frac{\Delta V_P}{\bar{V}_P} + \Delta\varepsilon_f\cos^4\psi + \Delta\delta_f\sin^2\psi \times \cos^2\psi + \Delta\varepsilon_b\right\}\sin^2\theta\tan^2\theta. \tag{10}$$

Here, $I \equiv \rho V$ is acoustic impedance, ρ is rock density, V_P and V_S are vertical P- and S-wave velocities, and differences $\Delta U \equiv \Delta I, \Delta V_P, \Delta V_S, \Delta\mu, \Delta\delta, \Delta\varepsilon$ and $\Delta\gamma$ are defined as deviations from an averaged medium parameter $\bar{U}$ using expressions $U_1 = \bar{U}[1 - \Delta U/(2\bar{U})]$ and $U_2 = \bar{U}[1 + (\Delta U/2U)]$, where $U \equiv I, V_P, V_S \ldots$. Indices 1 and 2 correspond, respectively, to media above and below the reflector when the incident wave comes from above.

The effective stress dependence of reflectivity in equation (10) is defined using expressions (2), (3), and (7)–(9).

COMPARISON WITH EXPERIMENTAL DATA AND ELLIPSOIDAL FRACTURE MODEL

Experimental data.—As the most appropriate, I use measured dependencies $V_P(p)$ and $V_S(p)$ for a dry sandstone sample with fractures developed artificially prior to the measurements by applying triaxial stress with an x_3 component much

Downloaded 11/03/15 to 130.56.64.29. Redistribution subject to SEG license or copyright; see Terms of Use at http://library.seg.org/

less than the rock strength limit and with x_1 and x_2 components essentially exceeding the limit (Sayers, 2002; his Figures 7 and 8). The resulting fractures prove to align normally to the x_3-direction. I calculate velocities V_P and V_S of P- and S-waves, propagating perpendicular and parallel to fracture faces, from expressions (2), (3), and equations

$$V_P = \left\{[(Z_{0P} + Z_N)^{-1} + \left(\frac{4}{3}\right)(Z_{0S} + Z_T)^{-1}]\rho^{-1}\right\}^{1/2}, \tag{11a}$$

and

$$V_S = [(Z_{0S} + Z_T)^{-1}\rho^{-1}]^{1/2}, \tag{11b}$$

true by definition. Here, ρ is rock density, Z_N and Z_T are fracturing-induced compliances, and Z_{0P} and Z_{0S} are compressive and shear compliances of the intact rock. Definitions $K^* = \rho(V_{0P}^2 - 4V_{0S}^2/3)$, $\mu^* \equiv \mu = \rho V_{0S}^2$, $E^* = 9\mu K^*/(\mu + 3K^*)$ and $\nu^* = (3K^* - 2\mu)/[2(3K^* + \mu)]$ were used to obtain the reference set of intact rock moduli (Table 1) from values $V_{0P} = 4400$ m/s and $V_{0S} = 2900$ m/s, determined in Sayers (2002) as characteristic for the intact rock sample near its strength limit at which the intergrain discontinuities that existed at lower stress are assumed to be closed.

Taking advantage of the proposed model [equations (1)–(9)] capability of covering a full range of void shapes from isometric (equant pores) to infinitesimally thin (fractures), I use equations (2) and (3) for modeling both Z_{0P} and Z_{0S} of intact rock and Z_N and Z_T from fractures. Compliances Z_{0P} and Z_{0S} are modeled by setting $e = 1$ and $c = 1$, which reduces the model to a random packing of spheres, while Z_N and Z_T are calculated using values $c_0 = 4$, $m = 0.25$, and $e = 0.025$ chosen [within limits of equation (6)] to ensure the best fit to experimental velocities V_{33} and V_{11} (P-waves perpendicular and parallel to fracture planes), $V_{12} = V_{21}$ (S-waves with both propagation and polarization parallel to fracture planes), and $V_{23} = V_{32} \approx V_{13} = V_{31}$ (S-waves with either propagation or polarization perpendicular to fracture planes). According to equation (8), velocities V_{11}, V_{22}, and $V_{12} = V_{21}$ are unaffected by fractures normal to x_3, and their dependence on confining stress is totally attributable to decrease of intergrain discontinuities, as if there are no fractures at all. Respectively, I set compliances Z_N and Z_T in expressions (11) to zero for these directions. Velocities V_{33} and $V_{23} = V_{32} \approx V_{13} = V_{31}$ influenced by fracturing are predicted using for Z_{0P} and Z_{0S} the same values as in calculations of V_{11}, V_{22}, and $V_{12} = V_{21}$.

The results are in reasonable agreement with experiments (Sayers, 2002) for the full range of 5 MPa $\le p \le$ 70 MPa of the stress applied to the fractured sample (Figure 1). This validates the model explicitly. The divergencies $V_{11} \neq V_{22}$ (solid and open circles in Figure 1a) and $V_{23} = V_{32} \neq V_{13} = V_{31}$ (open symbols in Figure 1b) between observed velocities reflecting imperfection of the experiment are not modeled as caused by an unidentified reason (e.g., nonideal isotropy of intact rock, nonideal alignment of fracturing, or imperfect contact of transducers).

Ellipsoidal crack model.—I reduce this comparison to establishing relations between anisotropy coefficients, defined in the models compared, because anisotropy is the most characteristic seismic feature of rocks with aligned fractures. For anisotropy coefficients of rocks with ellipsoidal cracks, I use equations (2) in Thomsen, (1995). In my designations, these equations read

$$\varepsilon_f^{ell} = \frac{8}{3}\frac{(1 - \nu^{*2})(1 - 2\nu)}{(1 - \nu^{*2})(1 - 2\nu^*)}\left(1 - \frac{K_f}{K_s}\right)\frac{K}{K^*}e^{ell}D_1 \tag{12a}$$

and

$$\gamma_f^{ell} = \frac{8}{3}\frac{(1 - \nu^*)}{(2 - \nu^*)}e^{ell}. \tag{12b}$$

To compare equations (9) and (12), the difference in definitions of fracture densities e and e^{ell} for the two models is taken into account. For this, both e and e^{ell} are expressed via fracture porosity as a universal parameter taken the same for both models, using expression (4) here and equation (3b) from Thomsen (1995). This results in the relation $e \approx 4(b/a)e_{ell}$, where b/a is the average aspect ratio of an ellipsoidal crack. With the use of this relation, setting, as in Thomsen (1995), $\nu^* = 0.25$, $\nu^* = 0.32$, $K^* = 5.6$ GPa, $K = 9.5$ GPa and choosing $c_0 = 5$, $p_1 = 5$ MPa, and $m = 0.35$, it can be shown that for dry voids, conditions $\varepsilon_f = \varepsilon_f^{ell}$ and $\gamma_f = \gamma_f^{ell}$ are satisfied at $p \approx 2.4$ MPa if $b/a = 0.0036$ (as in Thomsen, 1995), at $p \approx 11$ MPa if $b/a = 0.01$, and at $p \approx 33$ MPa if $b/a = 0.03$. For wet voids, the numbers are practically the same, and hydraulic connectivity manifests itself in rocks with rough-face fractures in about the same degree as in rocks with ellipsoidal fractures. Hence, for fixed effective stress values, the two models are mutually consistent. Note, however, that these fixed values belong to the stress interval where gradients of dependencies $\varepsilon_f(p)$ and $\gamma_f(p)$ are rather high, which restricts the applicability of stress-independent models such as equation (12) in real situations with variable effective stress.

The model in equations (1)–(9) is not applicable to the background anisotropy, caused by fine layering and/or mineral grain alignment. If, however, the background VTI is induced by bedding-concordant fracturing, then respective coefficients ε_b, δ_b, and γ_b are described by the right-hand sides of expressions (7), where parameters c and e relate to the VTI-inducing fracturing and p is the vertical component of effective stress.

Table 1. Input, calculated, and arbitrarily assigned parameters. The first three lines denote the first set; the bottom three lines denote the second set.

Input parameters	Calculated parameters		Parameters adapted (first set) or assigned arbitrarily (second set)				
$V_{0P}^* = 4400$ m/s	$K^* = 16.34$ GPa	$E^* = 37.51$ GPa	—	c_0	4	e	0.025
$V_{0S}^* = 2900$ m/s	$\mu^* = 16.78$ GPa	$\nu^* = 0.117$	—	p_1, MPa	5	m	0.35
$\rho^* = 400$ kg/m^3	—	—	—				
$V_{0P}^* = 3200$ m/s	$K^* = 10.0$ GPa	$E^* = 19.3$ GPa	$K_{f,w} = 2.00$ GPa	$\rho_{f,w}$, kg/m^3	1000	e	0.1
$V_{0S}^* = 2000$ m/s	$K = 19.0$ GPa	$\nu^* = 0.18$	$K_{f,gas} = 0.15$ GPa	$\rho_{f,gas}$, kg/m^3	300	m	0.35
$\rho^* = 2050$ kg/m^3	$\mu^* = 8.2$ GPa	$\rho = 740$ kg/m^3	$K_s = 36.0$ GPa	p_1, MPa	5	c_0	5

Downloaded 11/03/15 to 130.56.64.29. Redistribution subject to SEG license or copyright; see Terms of Use at http://library.seg.org/

MODEL-BASED PREDICTIONS

Fracture porosity

As in more complex models (Gangi, 1981), fracture porosity ϕ_c given by equation (4) decreases with increasing stress quickly, especially for large values of c_0 (Figure 2a). The gradient of the porosity dependence on stress decreases with m at $c_0 < 5$ and increases with m at $c_0 > 5$ (Figure 2b). The more concordant the fracture faces, the higher the parameter m and the faster the fractures close under compressive stress. This complies with experimental data (Kragelskii and Mikhin, 1984).

Seismic response

Dependencies $Z_N(p)$ and $Z_T(p)$ are calculated directly from equations (2a) and (2b), velocities $V_P(p)$ and $V_S(p)$, anisotropy coefficients, and reflectivity from equations (7), (9), and (10), respectively. Initial data are represented this time by averaged observed values of P- and S-wave interval velocities V^*_{0P}, V^*_{0S}, and density ρ^* in gas-filled Neocomian reservoirs of western Siberia (Avchyan, 1972) at depths of 2 to 3 km. Transfer to parameters for water-saturated rocks is done by a fluid substitution technique (e.g., Mavko and Mukerji, 1995); numerical values of densities $\rho_{f,gas}$, $\rho_{f,w}$ and bulk moduli $K_{f,gas}$, $K_{f,w}$ of pore gas and pore water at depths of 2 to 3 km are taken from Batzle and Wang (1992). Parameters c, K_s, ϕ, and η_c are chosen arbitrarily (see Table 1). For convenience, the parameters in Table 1, derived from Sayers (2002) and Avchyan (1972), are called first set and second set, respectively.

Effective pressure coefficient n is set to unity, so actually differential stress is considered. However, the term effective stress is used to remind one of the necessity of accounting for deviations of the coefficient n from unity.

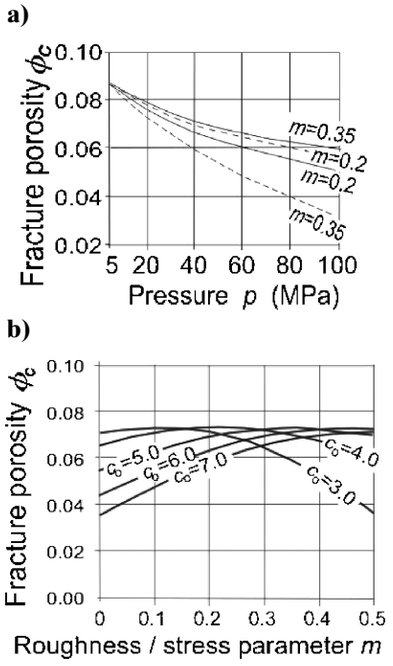

Figure 2. (a) Model dependence $\phi_c(p)$ of fracture porosity on effective stress at $m = 0.2$ and $m = 0.35$ for $c_0 = 3$ (solid lines) and $c_0 = 5$ (dashed lines) and (b) function $\phi_c(m)$ at $p = 60$ MPa. Fracture density $e = 0.1$, Young's modulus $E = 30$ GPa, and cohesion $p_1 = 5$ MPa.

Seismic velocities.—The model [equations (2)–(9)] reflects all of the generally recognized theoretical predictions and experimental data related to dependencies of the fractured rock velocities on external stress. Also, it reveals certain new aspects. First, at constant effective stress, the presence of connected equant porosity affects velocities in rocks with rough-face fractures the same way as in the case of (connected) ellipsoidal fractures: in the surface seismic frequency range, the P-wave velocity in wet rocks increases substantially with the decrease of the pore connectivity, while the S-wave velocity does not react on the pore connectivity variations (Figure 3). The difference in P-wave velocity resulting from the difference in equant pore connectivity decreases with effective stress p insignificantly.

Second, the diagnostic power of the relation V_P/V_S (and, hence, of the Poisson ratio) as a pore fluid type indicator for fractured rocks is considerable over a wide range of the stress p. It is especially strong at low p but decreases with the increase of pore connectivity (Figure 4).

Third, for dry fractures at $\phi = 0$, the model relation Z_N/Z_T, defined by equation (A-4b), is fixed, independent of stress p, and equals the relation $(1-\nu^*)/(1-\nu^*/2)$ prescribed by the mere linear slip deformation concept (Schoenberg and Sayers, 1995). However, it is not so for fractured rock with considerable equant porosity: the model predicts strong inequality $Z_N \ll Z_T$ not only for liquid, but also for gaseous pore fill having essentially nonzero incompressibility $K_{f,gas}$. The relation Z_N/Z_T increases with stress p but never surpasses the vacuum dry case limit $(1-\nu^*)/(1-\nu^*/2) < 1$ (Figure 4a). Respectively, V_P/V_S decreases with stress p. Since equation (3a) is valid for the seismic frequency range only, and at Thomsen's (1995) moderately high frequencies is to be replaced by equation (3b), the relation V_P/V_S in fractured rocks is implicitly frequency dependent because of the frequency dependence of the connected equant porosity effect on compliance Z_N in wet rocks.

Fourth, the effect of the pore fluid type on compliances Z_N and Z_T, predicted for a fixed stress p, agrees well with

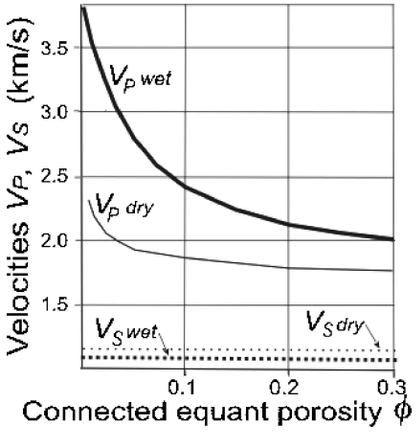

Figure 3. Velocities V_P (lines) and V_S (dots) as functions of connected equant porosity ϕ_c for dry (thin lines/dots) and wet (thick lines/dots) pores and fractures. Note the fast decrease of V_P with ϕ_c, especially for liquid-saturated rocks, and the independence of V_S of the pore connectivity.

Downloaded 11/03/15 to 130.56.64.29. Redistribution subject to SEG license or copyright; see Terms of Use at http://library.seg.org/

the result obtained using stress-independent models (e.g., Thomsen, 1995). The familiar pattern may change, however, if there is a significant lateral gradient of pore pressure within the reservoir. Indeed, decreased pore pressure in the hydrocarbon-producing part of a reservoir as compared to the waterflooded part is quite common. According to equations (2), the nonzero increment Δp_f influences not only normal compliance Z_N but shear compliance Z_T as well. Neglecting this influence leads to an apparent violation of the notion of shear modulus μ independence of the pore fluid type, which is the cornerstone of the fluid substitution principle and AVO-based discrimination between pore fluid types. To a lesser degree, this observation can be related to connected equant pores as well. An especially strong effect can be observed in the case of intense gas production for which a strong inequality $p_{f,gas} < p_{f,water}$ between gas- and water-saturated parts of a reservoir is characteristic. The generally accepted rule $\mu^* = \mu$ and $Z_T^* = Z_T$ for gas- and water-filled parts of the reservoir certainly does not hold in this case.

The magnitude of the effect can be evaluated assuming $\Delta p_f \equiv p_{f,water} - p_{f,gas} = 5$ MPa and the horizontal component of the stress $p \equiv |p_0 + p_1|_{hor} - p_f = 5$ MPa. The latter value is a reasonable estimate for p at a rather wide range of depths: 1 km $< z <$ 2.5 km (Figure 5), assuming minimum horizontal stress to be about one-half to one-third of lithostatic stress. (This relation is characteristic for gas reservoirs in the northern part of western Siberia.) For parameters shown in Table 1, the increment ΔV_S can then exceed 100 m/s (see Figure 6). Such a difference in shear-wave velocity can essentially affect AVO attributes used as fluid saturation indicators. The effect increases with parameters e, c, and p_f (i.e., it is especially strong at abnormally high pore pressure) and decreases with minimum horizontal effective stress component p. Note that the latter tends to increase with depth much slower than the vertical component of effective stress, as illustrated by Figure 6. Similar results are obtained by modeling the state of stress on a local (western Siberia, Volgo-Ural province) and regional (offshore Louisiana) scale (Lowrie et al., 2002).

Special care should be taken when interpreting AVO attributes in the course of time-lapse studies. The magnitude and position of maximum pore pressure gradients between hydrocarbon-producing and waterflooded parts of a reservoir can change in time significantly enough to influence the AVO inversion results.

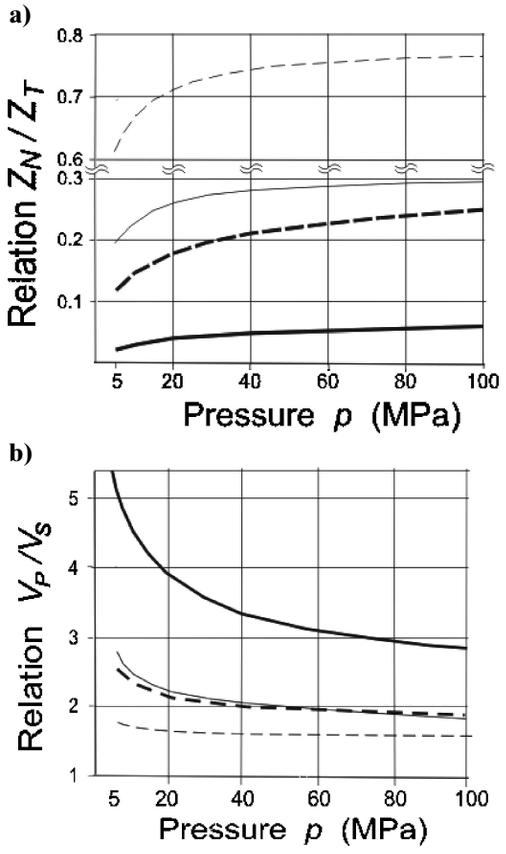

Figure 4. Relations (a) Z_N/Z_T and (b) V_P/V_S as functions of effective stress normal to the fracture faces. Note the essential decrease of Z_N/Z_T and increase of V_P/V_S with the stress for gas-filled fractures and equant pores. Designations as in Figure 3.

Anisotropy.—As in other models, all anisotropy coefficients ε_f, δ_f, and γ_f are negative, are linear in fracture density (or fracture porosity), and decrease in absolute value with stress rather quickly. Values $|\varepsilon|$ and $|\delta|$ are 1.5 to 5 times bigger for the dry case as compared to the wet case. Coefficient γ_f depends neither on the fracture (and equant pore) saturation nor on the value of equant porosity. Several new aspects arise. First, in dry rock, connected porosity ϕ does not affect anisotropy, while in wet, it does. The increase of connected equant porosity decreases the effect of diverse saturation on $|\varepsilon|$ values (Figure 7). Coefficient γ is not affected by pore fluid type or equant porosity if pore pressure does not change; δ behaves like ε.

Second, pore pressure variations affect not only ε and δ coefficients but γ coefficient as well (Figure 8). This leads to apparent violation of the notion of coefficient γ independence

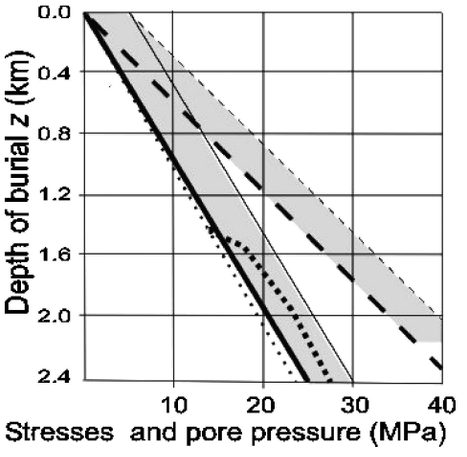

Figure 5. Schematic depth dependence of the lithostatic stress components and pore pressure. Shaded area marks the rock cohesion p_1 range. The pore pressure (small dots—hydrostatic; large dots—abnormally high) is commonly much less than the vertical component (dashed line) of the lithostatic stress but can be nearing its horizontal component p, especially at the zero cohesiveness p_1 (thick solid line).

of the pore fluid type, if pore pressure changes when crossing the gas–water contact (which is characteristic of gas-producing reservoirs), but these changes are neglected. Interestingly, absolute alteration of pressure affects γ much less than ε, while relative variations of all these coefficients are nearly the same (Figure 8); δ behaves like ε.

Finally, even at rather small fracture porosity $\phi_c = 0.005$, at pressure $p < 20$ MPa, all three anisotropy coefficients for the dry case and roughness $c \geq 3$ exceed in absolute value the limit of weak anisotropy defined as 0.1 (Thomsen, 1986).

Reflectivity.—The effect of the stress state on the reflectivity of a boundary between media with different fracturing is a rather complex function of many parameters [equation (13)]. To ease the analysis of the calculation results, (1) velocities and densities in wet host rocks above and below the reflector are set the same for equant porosity $\phi = 0.01$ above and $\phi = 0.25$ below the reflector; (2) only two characteristic values of the stress p are considered: $p_{min} = 5$ MPa and $p_{max} = 40$ MPa; and (3) only the results for isotropy and symmetry ray planes are shown. As in other models for aligned fracturing, the isotropy curves are insensitive to stress p, whereas in all symmetry cases considered the effect of stress variations on the $R(\theta)$ curve gradient (i.e., AVO gradient) is essential. Nontrivial predictions are as follows.

First, the difference in $R^{SYM}(\theta)$ gradients for $p = p_{min}$ and $p = p_{max}$ is about the same as the difference in the gradients for dry ($S_w = 0$) and wet ($S_w = 100\%$) cases. In contrast, the difference in $R^{SYM}(\theta)$ curve intercept is negligible for different p and quite strong (at considerable porosity ϕ) for different saturation (Figure 9). This can help distinguish the effects of saturation and effective stress (pore pressure) variations.

Second, connected equant porosity is one of the main features affecting both AVO intercept and gradient: increase of ϕ leads to decrease of the gradient absolute value, and vice versa. For the same fracture porosity, at large ϕ, the difference

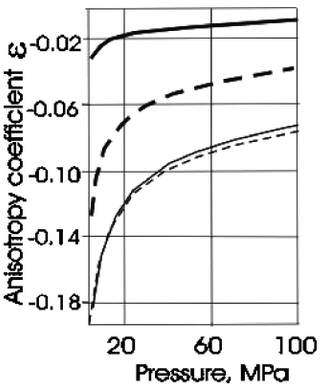

Figure 7. Anisotropy coefficients ε and γ as functions of stress p in wet (thick lines) and dry (thin lines) rocks. For ε, solid lines are for $\phi = 0.01$, and dashed lines are for $\phi = 0.25$. As seen, equant porosity does not affect ε in dry rocks, while in wet rocks the effect is rather strong; δ behaves like ε, and γ depends on neither ϕ nor pore fluid type.

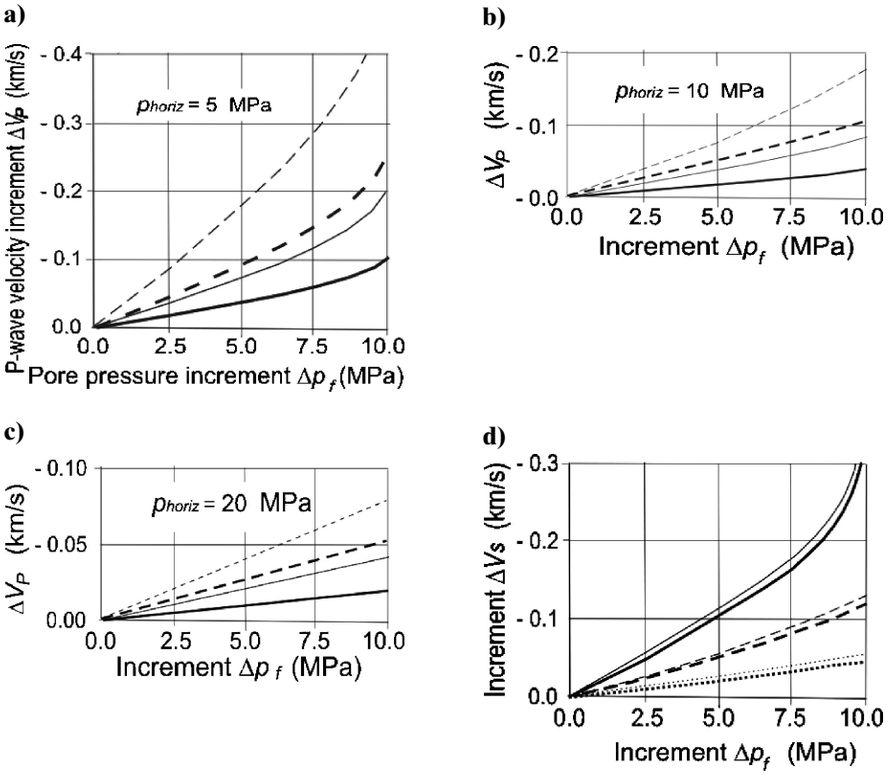

Figure 6. Increments dV_P of P-wave velocity at horizontal component of lithostatic stress where p equals (a) 5 MPa, (b) 10 MPa, and (c) 20 MPa. (d) Increment dV_S of S-wave velocity at $p = 5$ MPa. Functions of increment dp_f of pore pressure.

Downloaded 11/03/15 to 130.56.64.29. Redistribution subject to SEG license or copyright; see Terms of Use at http://library.seg.org/

between isotropy and symmetry gradients is large (Figures 9a,c); at small ϕ, this difference is small (Figures 9b,d). Note the isotropy gradient sign change because of VTI anisotropy in the lower (reservoir) layer at large ϕ (Figure 9c) but no change occurs at small ϕ (Figure 9d). Hence, at laterally stable VTI anisotropy, the particulars of gradient for isotropy and symmetry cases can help detect equant porosity lateral variations.

Finally, the effect of lateral pore pressure variations on reflectivity is similar to the effect on anisotropy coefficients.

A note of caution: The modeling results discussed here are related exclusively to the case of initially aligned fractures. Also, compliances and velocities were modeled for raypaths normal to fracture planes. If initially there was no fracturing, the fractures are not parallel, or raypath directions are away from the TI model axis of symmetry, then the effect of alteration of principal effective stress components may differ quantitatively from what is described here.

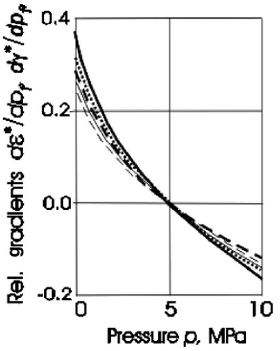

Figure 8. Relative gradients $d\varepsilon^*/dp_f$ and $d\gamma^*/dp_f$, $\varepsilon^* = \Delta\varepsilon/\varepsilon$ and $\gamma^* = \Delta\gamma/\gamma$, of anisotropy coefficients ε and γ as functions of the minimum horizontal component of effective stress. The range $0 < p \leq 10$ MPa is characteristic for a wide range of depths (down to 2 km and more, Figure 5). Note the strong effect of pore pressure on anisotropy and the uniformity of ε and γ relative gradients. Designations are as in Figure 7; δ behaves like ε.

CONCLUSION

Anisotropic effective stress dependencies of seismic velocities and reflectivity of rocks with aligned rough-face fractures and hydraulically connected equant porosity are represented by a simple model with a single stress-dependent parameter of fracture face roughness. The model adequately describes known effects of fluid saturation, pore-space connectivity, and pore pressure, and it also highlights some effects that had not attracted the attention of seismologists earlier. In particular, using the model the following are shown.

1) an apparent violation of the basic principle of the fluid substitution concept—the equality $\mu^* = \mu$ of shear modulus in gas- and water-saturated parts of a reservoir—can be observed if pore pressure in these parts is not the same, which

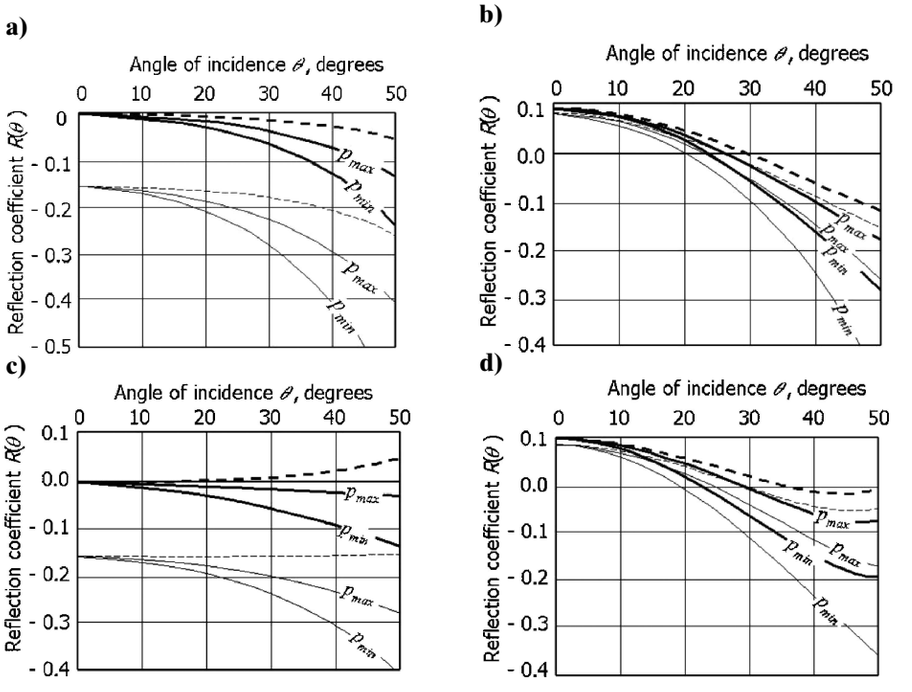

Figure 9. Curves $R(\theta)$ for ray planes parallel (SYM) and normal (ISO) to the HTI axis of symmetry at $p_{min} = 5$ MPa and $p_{max} = 40$ MPa. Layer 1 (seal): wet, $\phi = 0.01$, VTI with $\varepsilon_b = 0.08$, $\delta_b = 0.07$. Layer 2 (reservoir): wet (thick lines) or dry (thin lines), $\phi = 0.25$ (a, c) or $\phi = 0.01$ (b, d); no VTI (a, b) or VTI with $\varepsilon_b = 0.08$, $\delta_b = 0.07$ (c, d), HTI with coefficients ε_f, δ_f, and γ_f picked for p_{min} and p_{max} from Figure 7. As seen, the effect of pressure change on the $R(\theta)$ curve gradient is about the same magnitude as the effect of pore fluid replacement.

Downloaded 11/03/15 to 130.56.64.29. Redistribution subject to SEG license or copyright; see Terms of Use at http://library.seg.org/

is a typical situation for gas-producing fields. To avoid possible misinterpretation of AVO fluid saturation attributes, the state of pore pressure should be tracked carefully.

2) Comparison of 3D AVO intercept and gradient variations in the symmetry direction can help distinguish the effects of fluid substitution and effective stress (pore pressure) variations.
3) The increase of connected equant porosity decreases the effect of diverse saturation on coefficients ε and δ values but increases the difference between isotropy and symmetry estimates of 3D AVO gradient. Hence, at laterally invariant saturation in reservoirs with azimuthally aligned fracturing, the difference can point at lateral variations in equant porosity and help discriminate connected equant porosity from a disconnected one.
4) At intervals with small minimum horizontal effective stress (<5 MPa), the anisotropy of rocks with azimuthally aligned fractures increases drastically, which cannot be predicted by stress-independent models. The decrease of effective stress p (e.g., from abnormally high pore pressure) will amplify all of the above effects caused by fracturing-induced anisotropy, so it should be taken into account during interpretation.

The modeling also has led to some theoretically meaningful nontrivial results such as distinct effective stress dependence of relation Z_N/Z_T (and, hence, V_P/V_S), implicit frequency dependence of V_P/V_S for liquid-saturated fractured rocks with considerable connected equant porosity, and unification of relative gradients of all three Thomsen anisotropy coefficients as functions of horizontal effective stress component p.

Summarizing, when the state of stress does not vary laterally, the proposed model reflects particulars of the effect of fracturing on results of velocity and AVO analysis as adequately as models with ellipsoidal fractures do, so any one of the two models can be used. If, however, variations of effective stress (including pore pressure) are essential, the rough-face fracture model is the tool of choice.

The model's predictions are restricted to Hook's range of stress-deformation dependence, single system of strictly aligned fractures, negligible attenuation, and effective stresses $p > 0$. The observance of these restrictions in real media cannot be guaranteed. Hence, the model requires calibration when applied to practical cases. The best parameter for flexible calibration seems to be the fracture roughness c. As for the case of $p \to 0$, a more complicated stress-dependent model should be used.

ACKNOWLEDGMENTS

The author thanks Paradigm Geophysical for permission to publish this paper. He is also grateful to A. F. Gangi, who brought to notice his papers on the bed of nails model, to other reviewers, and to Allen Lowrie and Roger Haines for valuable corrections and comments. The work was partially supported by RFBR 03-05-65015.

APPENDIX A

COMPLIANCE OF DRY FRACTURES

Relative decrease $\Delta/2R \equiv \xi$ of the separation between centers of two contacting half-spherical asperities of equal radii R, pressed together with the force F, is expressed via Hertz's formalism (Timoshenko and Goodier, 1951):

$$\xi = \left(\frac{a}{R}\right)^2 = \sqrt[3]{\frac{9(1-\nu^2)^2F^2}{16E^{*2}R^4}}, \qquad \text{(A-1)}$$

Here, a is radius of the half-sphere contact (Figure A-1a). Quantities E^* and ν^* are defined in the main text.

In the model discussed, the distribution of asperities on the fracture face is assumed to be random and defined by an average distance cR between nearest asperity centers. Judging from porosity values of some packings of spheres (e.g., Bourbie et al., 1987, their Table 1.2), the distribution nearest to a random is a simple hexagonal pack. For the latter, the force F applied to a single asperity is related to area $S = 2\sqrt{3}c^2R^2$ (see Figure A-1), so

$$F = 2\sqrt{3}c^2R^2p, \qquad \text{(A-2)}$$

where p is effective stress. For fractures, normal to the load F, substitution of equation (A-2) into equation (A-1) yields

$$\xi = \left(\frac{a}{R}\right)^2 = \frac{3}{2}c\sqrt[3]{2c\left[(1-\nu^{*2})\left(\frac{f}{E^*}\right)\right]^2}. \qquad \text{(A-3)}$$

According to White (1983), compliance of a fracture with rough faces is defined as $Z_N^0 = (d\Delta/dp)$. For a series of parallel fractures with average spacing L, the fracture density can be defined as $e = 2R/L$, and the additional normal compliance Z_N imparted to the rock by the fractures can be expressed

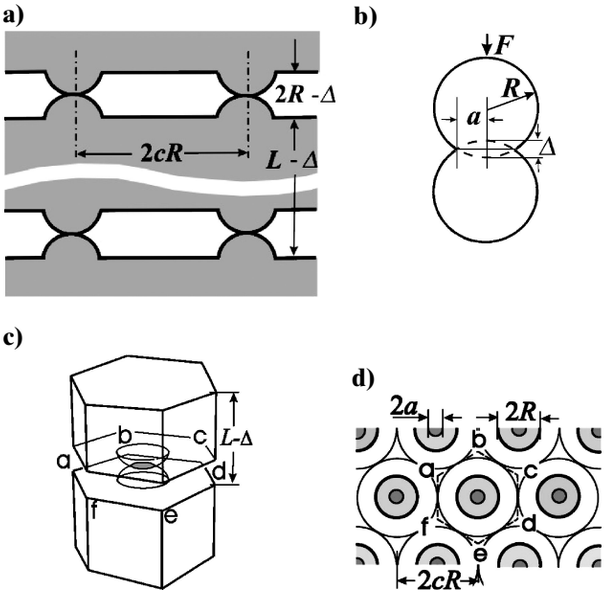

Figure A-1. Fractured rock model with hexagonal grid of asperities on fracture faces: (a) Hertzian contact of elastic spheres. (b) Fracture plane view. (c) Normal section view; dark cycles are contacts of asperities belonging to opposite fracture faces. (d) Isometric view of the hexagonal prism *abcdef* as an element constituent of the fractured rock model.

Downloaded 11/03/15 to 130.56.64.29. Redistribution subject to SEG license or copyright; see Terms of Use at http://library.seg.org/

Downloaded 11/03/15 to 130.56.64.29. Redistribution subject to SEG license or copyright; see Terms of Use at http://library.seg.org/

(e.g., Schoenberg and Sayers, 1995) as $Z_N = Z_N^0 e$. Assuming e independent of, or slowly varying with, stress p and differentiating equation (A-3) yields

$$Z_N = ce\frac{1}{\mu}\sqrt[3]{\frac{c}{3}\frac{(1-\nu^*)^2}{(1+\nu^*)}\frac{E^*}{p}}. \qquad \text{(A-4a)}$$

To obtain an analogous equation for tangential compliance Z_T, recall that the only kind of shear stress p' allowed by the model considered is that resulting from wave propagation. This stress is superimposed on a background effective stress p, deforming the asperity contact areas. Shear stress tangential to fracture planes induces tangential deformations Δ' (Figure A-1b). By analogy with the derivation of expression (A-4a), using this time the definition $Z_T = (1/L)(d\Delta'/dp')$ for the sequence of dry fractures, the differentiation yields

$$Z_T = ce\frac{2-\nu^*}{2\mu}\sqrt[3]{\frac{c}{3}(1-\nu^{*2})^{-2}\frac{E^*}{p}} = Z_N\frac{2-\nu^*}{2(1-\nu^*)}. \qquad \text{(A-4b)}$$

APPENDIX B

COMPLIANCE OF SATURATED FRACTURES

To transfer to the case of saturated fractures hydraulically connected with equant pores (if any), the starting point is equation (A-25) in Thomsen (1995),

$$\frac{1}{\bar{K}} = \frac{1}{K} + \left(1-\frac{K_f}{K_s}\right)\phi_c\left\langle\frac{\varepsilon^c_{mm}}{-\bar{p}}\right\rangle^* D. \qquad \text{(B-1)}$$

The fluid influence factor D takes different forms for different frequency ranges. As follows from equations (5a), (5b), and (A26b) in Thomsen (1995) for relatively low frequencies characteristic for surface seismic, when the fluid pressure has time to equilibrate locally between fractures and adjacent connected pores,

$$D \equiv D_1 = \left\{1-\frac{K_f}{K_s}+\frac{K_f}{\phi}\left[\left(\frac{1}{K^*}-\frac{1}{K_s}\right)+\phi_c\left\langle\frac{\varepsilon^c_{mm}}{-\bar{p}}\right\rangle^*\right]\right\}^{-1}, \qquad \text{(B-2a)}$$

while at moderately high frequencies, when there is no essential fluid flow between cracks and pores,

$$D \equiv D_2 = \left\{1-\frac{K_f}{K_s}+K_f\left[\left(\frac{1}{K^*}-\frac{1}{K_s}\right)+\frac{1-\frac{K_f}{K_s}}{1-\frac{K_f}{K}}\left\langle\frac{\varepsilon^c_{mm}}{-\bar{p}}\right\rangle^*\right]\right\}^{-1}. \qquad \text{(B-2b)}$$

Here, $\bar{K}$, K, K_s, K_f, ϕ_c, and ϕ designate the same values as in the main text; ε^c_{ij}, $i=j=m$, is a component of the strain in the fractures, resulting from the far-field application of the average stress σ; and pressure $\bar{p}$ is defined as $\sigma_{mn}(jj) = -\bar{p}\delta_{mn}$, where δ_{mn} is the Kroneker delta.

Equations (B-1) and (B-2) have two remarkable features. First, they are derived with no specific restrictions on the fracture shape. Second, their term $\langle\varepsilon^c_{mm}/(-\bar{p})\rangle^*$ expressing the compliance of a fracture is the only component responsible for additional compliance of the rock because of fracturing, and it is precisely for the dry case, for which equations (A-4) are derived here.

Using these properties, I replace the term $\langle\varepsilon^c_{mm}/(-\bar{p})\rangle^*$ in equation (B-1) with the equation (A-4a) core related to a single fracture. Next, I relate the moderately high frequency fluid influence factor D_2 to the case of disconnected pores at low (seismic) frequencies, since in this case there is also no essential fluid flow between fractures and (disconnected) equant pores. Finally, taking into account that $(1/\bar{K})-(1/K)=(1/\bar{E})-(1/E)$ (Thomsen, 1995) and assuming $\bar{p}$ in Thomsen's (1995) notation be the same as p in my notation, I obtain equations (2b) and (3), setting the quantity D in equation (2b) to be the Voigt average of D_1 and D_2.

As to the tangential compliance Z_T, it is known (e.g., Thomsen, 1995) to be independent of fluid saturation, so equation (2a) is obtained by dropping the asterisks in equation (A-4b).

APPENDIX C

FRACTURE POROSITY

For the model considered, the volume of an elemental hexagonal prism enclosing area $\pi c^2 R^2$ of fracture around each asperity (Figure A-1d) is

$$\vartheta_{frac} = 2\sqrt{3}c^2R^2\times(2R-\Delta) = 4\sqrt{3}c^2R^3(1-\xi), \qquad \text{(C-1)}$$

while the volume of (indented) asperities within the prism is

$$\vartheta_{asp} = \frac{4}{3}\pi R^3 - \frac{1}{3}\pi\Delta^2(3R-\Delta) \approx \frac{4}{3}\pi R^3(1-3\xi^2). \qquad \text{(C-2)}$$

With account of expression (1), the total volume of the rock prism attributed to each fracture is

$$\vartheta = 2\sqrt{3}c^2R^2\times(L-\Delta) = 4\sqrt{3}c^2R^3\left[\left(\frac{1}{e}\right)-\xi\right]. \qquad \text{(C-3)}$$

By definition, porosity ϕ_p is the relation of total volume of rock pore space to rock volume. Hence,

$$\phi_p = \frac{(\upsilon_{frac}-\upsilon_{asp})}{\upsilon} = \frac{e}{1-e\xi}\left[1-\frac{\pi c^{-2}}{3\sqrt{3}}(1-3\xi^2)-\xi\right]. \qquad \text{(C-4)}$$

Equation (4) replicates expression (C-4), where factor $1-\phi_p = \pi/(3\sqrt{3}) \approx 0.605$ is replaced by 0.64 to make it consistent with porosity $\phi_p = 0.36$ of random packs defined in Bourbie et al. (1987, Table 1.2).

APPENDIX D

STRESS DEPENDENCE OF THE ROUGHNESS FACTOR c

I choose for this dependence the power law form advocated in Gangi (1981):

$$c = c_0\left(\frac{p_1}{p}\right)^m, \quad m \geq 0. \qquad \text{(D-1)}$$

The power m value can be fixed taking into account Kragelskii and Mikhin (1984) proportionality

$$S \propto p^k, \quad \frac{4}{5} \leq k \leq \frac{9}{10}, \qquad \text{(D-2a)}$$

established experimentally for total relative area S of asperity contacts. For the model considered, this area is

$$S \propto \left[\frac{a}{(cR)}\right]^2. \qquad \text{(D-2b)}$$

Replacing S in the latter relation by equation (D-2a) and (a/R) with the right-hand side of equation (A-3) and expressing parameter c by equation (D-1) yields $0.2 \le m \le 0.35$. Note that the model prescribes (unachievable) upper limit $m \to 0.5$ at $k \to 1$ when the decrease of separation ξ tends to zero because area S is still linearly increasing with stress p.

APPENDIX E

DERIVATION OF EQUATIONS (7)

As shown in Liu et al. (1996) and Kozlov (1997), elastic properties of models with rough-face fractures are consistent with the concept of linear slip interface (Schoenberg, 1983). In the framework of this concept, Schoenberg (1994) derives relations between aligned fracturing-induced compliances Z_N and Z_T and Lamé constants λ and μ of the intact medium, on one hand, and elements c_{ij} of Hooke's matrix for a rock with VTI symmetry on the other. In notation used here, these relations are $c_{66} = \mu$, $c_{55} = c_{44} = \mu/(1 + \mu Z_T)$, $c_{33} = \mu/(G + \mu Z_N)$, and $c_{13} = (1 - 2G)c_{33}$, $c_{11} = [1 + 4(1 - G)\mu Z_N]c_{33}$, where $G \equiv \mu/(\lambda + 2\mu) \equiv (V_S/V_P)^2$. Inserting these relations into expressions

$$\varepsilon'_f = \frac{c_{11} - c_{33}}{2c_{33}}, \qquad \text{(E-1a)}$$

$$\gamma'_f = \frac{c_{66} - c_{44}}{2c_{44}}, \qquad \text{(E-1b)}$$

and

$$\delta'_f = \frac{(c_{13} + c_{44})^2 - (c_{33} - c_{44})^2}{2c_{33}(c_{33} - c_{44})} \approx \frac{c_{13} + 2c_{44} - c_{33}}{c_{33}} \qquad \text{(E-1c)}$$

for generic Thomsen anisotropy coefficients (Thomsen, 1986; my notation is ε'_f, δ'_f, and γ'_f for such coefficients in HTI medium) yields equations

$$\varepsilon'_f = 2(1 - G)\mu Z_N, \qquad \text{(E-2a)}$$

$$\gamma'_f = \frac{\mu Z_T}{2}, \qquad \text{(E-2b)}$$

and

$$\delta'_f = \frac{2(1 - G)\mu(GZ_T - Z_N)}{1 - G + \mu(Z_T - Z_N)} \approx \frac{2\mu(Z_N - GZ_T)}{1 + \mu Z_T}, \qquad \text{(E-2c)}$$

which relate the anisotropy coefficients to shear modulus μ, relation G, and compliances Z_N and Z_T.

Inserting expressions (2) in to equations (E-2) defining compliances Z_N and Z_T for a rock with VTI symmetry and setting $G = 0.25$ [an appropriate value for clastic rocks; Thomsen (1986)] yields formulas (9).

REFERENCES

Avchyan, G. M., 1972, Physical properties of rocks at in situ conditions imitated in laboratory (in Russian): Nedra Press.

Bakulin, A., Grechka, V., and Tsvankin, I., 2000, Estimation of fracture parameters from reflection seismic data—Part II: Fractured models with orthorhombic symmetry: Geophysics, **65**, 1803–1817.

Batzle, M., and Wang, Z., 1992, Seismic properties of pore fluids: Geophysics, **57**, 1396–1408.

Boitnott, G. N., Biegel, R. L., Scholz., C. H., Yoshioka, N., and Wang, W., 1992, Micromechanics of rock friction 2: Quantitative modeling of initial friction with contact theory: Journal of Geophysical Research, **97**, 8965–8978.

Bourbie, T., Coussy, O., and Zinszner B., 1987, Acoustics of porous media: Editions TECHNIP.

Crampin, S., 1994, The fracture criticality of crustal rock: Geophysical Journal International, **118**, 428–438.

Gangi, A. F., 1981, The variation of mechanical and transport properties of cracked rock with pressure: U.S. Symposium on Rock Mechanics, Massachusetts Institute of Technology, Proceedings, 83–89.

Gangi, A. F., and Carlson, R. L., 1996, An asperity-deformation model for effective pressure: Tectonophysics, **256**, 241–251.

Greenwood, J. A., and Williamson, J., 1966, Contact of nominally flat surfaces: Proceedings of the Royal Society of London, Series A., **295**, 300–319.

Hudson, J. A., 1981, Wave speeds and attenuation of elastic waves in material containing cracks: Geophysical Journal of the Royal Astronomical Society, **64**, 133–150.

——— 2000, The effect of fluid pressure on wave speeds in cracked solid: Geophysical Journal International, **143**, 302–310.

Hudson, J. A., and Crampin, S., 2003, Comment on: "The 3D shear experiment over the Natih field in Oman: The effect of fracture-filling fluids on shear propagation" by C. M. van der Kolk, W. S. Guest and J. H. H. M. Potters: Geophysical Prospecting, **51**, 365–368.

Hudson, J. A., Liu, E., and Crampin, S., 1996, The mechanical properties of materials with interconnected cracks and pores: Geophysical Journal International, **124**, 105–112.

Kozlov, E. A., 1997, Reflection of seismic waves from loaded (fractured) layers with non-welded contacts: 67th Annual International Meeting, SEG, Expanded Abstracts, 2009–2012.

Kozlov, E. A., and Varivoda, D. Y., 2000, A model of fractured rock relating seismic anisotropy to the state of stress: 62nd Annual Conference, European Association of Geoscientists and Engineers, Extended Abstracts, P-31.

Kragelskii, V. I., 1965, Friction & wear: Butterworth, chapter 2.

Kragelskii, V. I., and Mikhin, N. M., 1984, Friction units in machines: (in Russian) Machinostroyeniye.

Liu, E., Li, X.-Y., and Zhang, Z., 2001, Sensitivity of interfacial compliances to fluid saturation and pore pressure: 63rd Conference, European Association of Geoscientists and Engineers, Extended Abstracts, P033.

Liu, E., MacBeth, C. D., Pointer, T., Hudson, D., and Crampin, S., 1996, The elastic complience of fractured rock: 66th Annual International Meeting, SEG, Expanded Abstracts, 1841–1845.

Lowrie, A., Kozlov, E. A., Khaydukov, V. N., Watkins, J., Garagash, I. A., Makarov, V. V., and Malyarova, T. N., 2002, 2D/3D geophysical modeling of Mesozoic onshore rocks and Tertiary offshore sediments: Annual Meeting, American Association of Petroleum Geologists, Extended Abstracts.

Mavko, G., and Mukerji, T., 1995, Seismic pore space compressibility and Gassmann's relation: Geophysics, **60**, 1743–1749.

O'Connell, R. G., and Budiansky, B., 1977, Viscoelastic properties of fluid-saturated cracked solids: Journal of Geophysical Research, **82**, 5719–5735.

Pecorari, C., 1997, Acoustoelasticity in cracked solids: Geophysical Journal International, **129**, 169–175.

Ruger, A., 1998, Variation of P-wave reflectivity with offset and azimuth in anisotropic media: Geophysics, **63**, 935–947.

Sayers, C. M., 2002, Stress-dependent elastic anisotropy of sandstones: Geophysical Prospecting, **50**, 85–95.

Schoenberg, M., 1983, Reflection of elastic waves from periodically stratified media with interfacial slip: Geophysical Prospecting, **31**, 265–292.

——— 1994, Transversely isotropic media equivalent to thin isotropic layers: Geophysical Prospecting, **42**, 885–915.

Schoenberg, M., and Helbig, K., 1997, Orthorhombic media: Modeling elastic wave behavior in a vertically fractured earth: Geophysics, **62**, 1954–1974.

Schoenberg, M., and Sayers, C., 1995, Seismic anisotropy of fractured rock: Geophysics, **60**, 204–211.

Thomsen, L., 1986, Weak elastic anisotropy: Geophysics, **51**, 1954–1966.

——— 1995, Elastic anisotropy due to aligned cracks on porous rock: Geophysical Prospecting, **43**, 805–830.

Timoshenko, S., and Goodier, J. N., 1951, Theory of elasticity, second ed.: McGraw-Hill Book Company.

Downloaded 11/03/15 to 130.56.64.29. Redistribution subject to SEG license or copyright; see Terms of Use at http://library.seg.org/

Tsvankin, I., 1997, Reflection moveout and parameter estimation for horizontal transverse isotropy: Geophysics, **62**, 614–624.
van der Kolk, C. M., Guest, W. S., and Potters, J. H. H. M., 2001, The 3D shear experiment over the Natih field in Oman: The effect of fracture-filling fluids on shear propagation: Geophysical Prospecting, **49**, 179–197.
Vernik, L., 1993, Microcrack-induced versus intrinsic anisotropy in mature HC-source shales: Geophysics, **58**, 1703–1706.
White, J. E., 1983, Underground sound: Application of seismic waves: Elsevier Science Publishing Company.

Downloaded 11/03/15 to 130.56.64.29. Redistribution subject to SEG license or copyright; see Terms of Use at http://library.seg.org/